JACS
JOURNAL OF THE AMERICAN CHEMICAL SOCIETY

Article

pubs.acs.org/JACS
Terms of Use CC-BY

Photochemical Pump and NMR Probe: Chemically Created NMR Coherence on a Microsecond Time Scale

Olga Torres, Barbara Procacci, Meghan E. Halse, Ralph W. Adams, Damir Blazina, Simon B. Duckett,* Beatriz Eguillor, Richard A. Green, Robin N. Perutz,* and David C. Williamson

Department of Chemistry, University of York, Heslington, York YO10 5DD, U.K.

Supporting Information

ABSTRACT: We report pump−probe experiments employing laser-synchronized reactions of *para*-hydrogen (*para*-H_2) with transition metal dihydride complexes in conjunction with nuclear magnetic resonance (NMR) detection. The pump−probe experiment consists of a single nanosecond laser pump pulse followed, after a precisely defined delay, by a single radio frequency (rf) probe pulse. Laser irradiation eliminates H_2 from either Ru$(PPh_3)_3(CO)(H)_2$ **1** or *cis*-Ru$(dppe)_2(H)_2$ **2** in C_6D_6 solution. Reaction with *para*-H_2 then regenerates **1** and **2** in a well-defined nuclear spin state. The rf probe pulse produces a high-resolution, single-scan ^{1}H NMR spectrum that can be recorded after a pump−probe delay of just 10 μs. The evolution of the spectra can be followed as the pump−probe delay is increased by micro- or millisecond increments. Due to the sensitivity of this *para*-H_2 experiment, the resulting NMR spectra can have hydride signal-to-noise ratios exceeding 750:1. The spectra of **1** oscillate in amplitude with frequency 1101 ± 3 Hz, the chemical shift difference between the chemically inequivalent hydrides. The corresponding hydride signals of **2** oscillate with frequency 83 ± 5 Hz, which matches the difference between couplings of the hydrides to the equatorial ^{31}P nuclei. We use the product operator formalism to show that this oscillatory behavior arises from a magnetic coherence in the plane orthogonal to the magnetic field that is generated by use of the laser pulse without rf initialization. In addition, we demonstrate how chemical shift imaging can differentiate the region of laser irradiation thereby distinguishing between thermal and photochemical reactivity within the NMR tube.

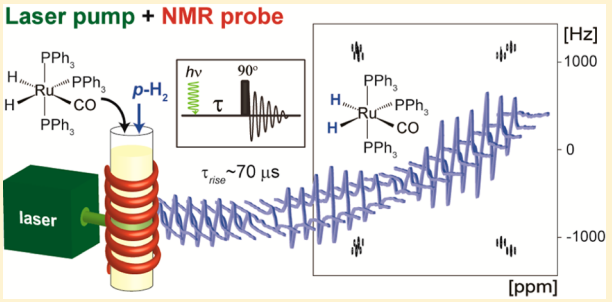

1. INTRODUCTION

Dynamic nuclear magnetic resonance (NMR) spectroscopy has numerous applications for studying chemical exchange phenomena in the steady state.[1] The exchange information is present in the free induction decay (FID), which is recorded for several hundred milliseconds. The exchange time scale accessible to line shape analysis is typically determined by the frequency difference between exchanging nuclei. Alternatively, exchange spectroscopy (EXSY) experiments are used for probing slower dynamic exchange, where the accessible time scales are determined by relaxation.[2] In practice, the need for good signal-to-noise ratios for accurate measurements plays a dominant role in determining the processes that can be followed. NMR spectroscopy can also be used to follow much slower reactions as they evolve, through a series of measurements at different times. Recently, flow methods, analogous to stopped-flow UV, have been introduced, which access faster time scales.[3,4]

In contrast, numerous pump−probe methods have been employed to study kinetics on much shorter time scales with the fast detection techniques of UV/vis absorption and emission,[5,6] IR,[7] and Raman spectroscopies.[8−10] In principle, NMR spectroscopy could be used in time-resolved pump−probe measurements if its sensitivity can be enhanced; laser pump−probe NMR spectroscopy might be expected to become a powerful tool given the complementary structural information on an NMR spectrum. Inspired by research on in situ laser photolysis and our experiments with *para*-hydrogen (*para*-H_2) hyperpolarization of NMR,[11−13] we have developed a time-resolved spectroscopy method using laser initiation and NMR detection and illustrate it for pump−probe delays as short as 10 μs.

In a standard NMR experiment, it is the Zeeman effect and the associated Boltzmann statistics that generate a bulk magnetic order. The magnitude of this bulk magnetization depends on a very small population difference and so gives rise to a weak NMR signal. This signal is detected following a radio frequency (rf) excitation pulse, which interacts with the bulk magnetization to produce a coherence in the plane orthogonal to the main magnetic field, which is then detected in the form of the FID. In the 14.1 T (600 MHz) magnetic field used here, the Zeeman effect produces a difference in nuclear-spin-state populations that is 1 for every 21300 ^{1}H nuclei present. Several hyperpolarization methods have been designed to improve the sensitivity of NMR by perturbing this population difference.

Received: May 12, 2014
Published: June 19, 2014

 © 2014 American Chemical Society dx.doi.org/10.1021/ja504732u | J. Am. Chem. Soc. 2014, 136, 10124−10131

Some notable examples include optical pumping of noble gases,[14−16] dynamic nuclear polarization,[17,18] and photochemically induced dynamic nuclear polarization (photo-CIDNP).[19−21] In the photo-CIDNP method, a spin-correlated radical pair is used to generate NMR signal enhancements on the order of 10^2. The photo-CIDNP approach has been used to observe short-lived radicals and to monitor reactivity on millisecond to second time scales.[22−25] In 1976, Ernst demonstrated that magnetic oscillations due to a chemically induced magnetic coherence can be observed if CIDNP is initiated coherently on a very short time scale.[26] A related chemically initiated magnetic coherence is exploited here in our time-resolved NMR spectroscopy method to give rise to NMR signal enhancements of several orders of magnitude that build up on microsecond time scales. In our method, we use the long-lived and readily prepared *para*-H_2 molecule, rather than a radical, as the source of hyperpolarization, creating the potential for high-sensitivity measurements.[27,28]

para-Hydrogen (*para*-H_2) is a reactive molecule in which the nuclear spins are aligned antiparallel as the linear combination $\alpha\beta-\beta\alpha$ and hence they exist in a pure singlet state. Upon reaction with *para*-H_2, products with nonequilibrium states give rise to highly enhanced NMR signals that have been used to probe chemical reactivity in many different ways. Bowers and Weitekamp were the first to recognize the potential for NMR hyperpolarization using *para*-H_2. In 1986, they predicted that if *para*-H_2 were used in a hydrogenation reaction, reaction products with a spin polarization on the order of unity could be created.[29] They later confirmed, experimentally, that under conditions where the symmetry of the molecular *para*-H_2 was broken through its transformation into chemically distinct proton environments in a product, signal enhancements in ^{1}H NMR spectra did indeed result.[30] Subsequently they refined their approach to differentiate chemical transformations that proceed in a strong magnetic field (parahydrogen and synthesis allow dramatically enhanced nuclear alignment, PASADENA)[30] from those proceeding in a low magnetic field prior to NMR detection in a strong magnetic field (adiabatic longitudinal transport after dissociation engenders net alignment, ALTADENA).[31] The term PHIP (*para*-hydrogen induced polarization) has also been used in the literature to describe these effects more generally.[32] Previous applications of PHIP have included detection of reaction products containing *para*-H_2-derived protons in catalytic studies and *in vivo*.[27,33−39] Refinements of these methods called one-proton PHIP and signal amplification by reversible exchange (SABRE) have also been described.[33,35,40]

para-Hydrogen hyperpolarization is most commonly described in the literature through the use of energy level versus population diagrams[41] with others favoring product operator notation.[42,43] It follows from the former description that when two new inequivalent proton environments (I and S) are created from *para*-H_2 in a reaction product they yield enhanced antiphase NMR signals because the resulting energy level overpopulations reflect *para*-H_2's original $\alpha\beta$ spin orientation (Figure 1a). The product operator representation of the initial state in such a product is the singlet: $-{}^1/_2(2I_xS_x + 2I_yS_y + 2I_zS_z)$, which is made up of a zero quantum coherence ($ZQ_x = {}^1/_2(2I_xS_x + 2I_yS_y)$) and the longitudinal two-spin-order term, ${}^1/_2(2I_zS_z)$.[43,44] It is interesting to note that organic systems have been prepared in related states by Levitt, Bodenhausen, and Warren without laser synchronization and have potential applications because they can be long-lived.[45−49] Indeed, such

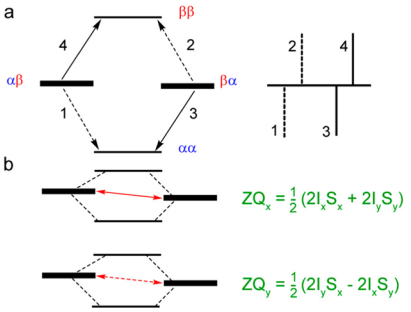

Figure 1. (a) Population-of-states model for a *para*-H_2-derived reaction product containing nuclei I and S, under PASADENA conditions with the resultant antiphase NMR peaks illustrated. (b) Representation of the non-NMR-detectable zero-quantum coherences with associated product operators for two spins I and S.[42]

long-lived states can also be generated by PHIP in symmetric organic molecules as shown recently.[50,51]

In a conventional high-field *para*-H_2-enhanced experiment,[30] the addition of *para*-H_2 occurs asynchronously, and the reaction time is long on the NMR time scale. Therefore, the amplitude of the ZQ_x coherence (and any associated terms) averages to zero (in the high field limit) and so the only observed transitions arise as a result of the longitudinal two-spin order term (Figure 1a). We seek here to probe the evolution of the *para*-H_2-derived magnetization in a new and efficient way, such that the enhanced signals can be monitored on microsecond time scales. To achieve this goal, we first need to prepare a well-defined starting state. We do this by using a laser pump pulse to initiate a reaction with *para*-H_2 photochemically (Figure 2a). Specifically, we use the light-

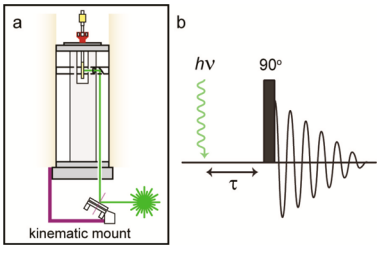

Figure 2. (a) Schematic of the laser irradiation system; the unfocused laser beam is reflected off the lower mirror into the probehead where a second mirror directs the beam onto the sample through a hole in the housing. (b) NMR pump−probe sequence used in this PHIP study.

induced electronic excitation of a transition metal complex to achieve prompt ligand dissociation. In fact, loss of H_2 occurs during the single 10 ns laser pulse, and *para*-H_2 therefore reacts with the unsaturated reaction intermediate in a time-precise and highly reproducible manner (Figure 3). We also need to consider carefully the behavior of the ZQ_x coherence, which is now created synchronously and subsequently evolves into ZQ_y (Figure 1b) during the pump−probe delay according to the chemical shift and J-coupling differences between the I and S proton environments (as demonstrated in section 2.2). This method is so reproducible that a series of measurements associated with a 2D-experiment can be collected. We follow the evolution of these magnetic states, the zero-quantum coherences, through the application of a probe NMR pulse (Figure 2b). Thereby, we collect diagnostic information about the product and, indirectly, learn about the reactivity of the

dx.doi.org/10.1021/ja504732u | J. Am. Chem. Soc. 2014, 136, 10124−10131

intermediate from which the product is formed. This differs from previous work where continuous irradiation in an NMR probe at low temperature has been used to build up the concentration of highly reactive species in order to enable their characterization; photoproducts such as alkane complexes reflect notable examples of this method.[12,52,53] The continuous irradiation approach has also been used with *para*-H_2 to observe new species.[54−56]

In the studies reported here, only a short section of the sample tube within the NMR detection coil is irradiated (Figure 2a),[11] and a further, longer section of the active volume of the coil is therefore unaffected by the laser beam. In a further technical development, we use this selectivity to differentiate the region of the NMR tube where the photochemical reaction occurs by making use of the NMR probe's gradient coil to perform chemical-shift imaging. In this case, we show that the enhanced signal is derived exclusively from the short irradiated region of the tube and hence demonstrate that thermal and photochemical activity can be distinguished.

Two types of ruthenium dihydride complex are used in this study: $Ru(PPh_3)_3(CO)(H)_2$ (**1**) and *cis*-$Ru(dppe)_2(H)_2$ (**2**) (Figure 3). They both undergo photochemical loss of H_2 on a

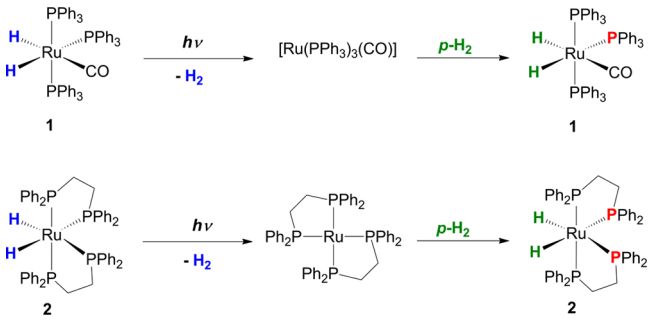

Figure 3. Photochemical reactivity of compounds **1** and **2** toward *para*-H_2 harnessed in this work. Blue denotes ^1H nuclei not derived from *para*-H_2, while green indicates hyperpolarized ^1H nuclei originating from *para*-H_2 oxidative addition. The phosphorus nuclei in red are the dominant source of the magnetic inequivalence of the hyperpolarized hydride nuclei in **2**.

picosecond time scale to generate $Ru(CO)(PPh_3)_3$ and $Ru(dppe)_2$ (dppe = $Ph_2PCH_2CH_2PPh_2$), respectively, before being reformed by reaction with hydrogen.[57−60] The kinetics of reaction of these intermediates with H_2 have been determined previously by time-resolved absorption spectroscopy; the time constants for recombination under 3 atm H_2 (as used here) are 1.4 and 4.8 μs, respectively. Consequently, >99.99% of the photoproducts have reacted with *para*-H_2 just 0.1 ms after the initial laser pulse, which makes them ideal candidates for this study.[57,58]

2. RESULTS

2.1. Laser Pump−NMR Probe Experiments. In our NMR pump−probe experiments, a *single* 10 ns laser pulse at 355 nm is followed by a precisely defined pump−probe delay, τ, and a *single* rf pulse (Figure 2b). The resultant free induction decay (FID) is collected over a period of 350 ms, in exactly the same way as for a traditional NMR experiment. In this study, the reaction products were stable on this time scale. The result is a high-resolution ^1H NMR spectrum that also encodes the evolution of any *para*-H_2-derived magnetic states during the pump−probe delay. In these studies, the sample consists of an optically dilute C_6D_6 solution of either **1** or **2**. In **1**, the two protons originating from *para*-H_2 are placed in chemically distinct hydride environments, while in **2** they are created chemically equivalent but magnetically inequivalent by virtue of phosphorus couplings. This is exemplified by the corresponding $^1H\{^{31}P\}$ pump−probe NMR spectra of **1** and **2** that are generated under *para*-H_2 shown in Figure 4. The ^1H NMR

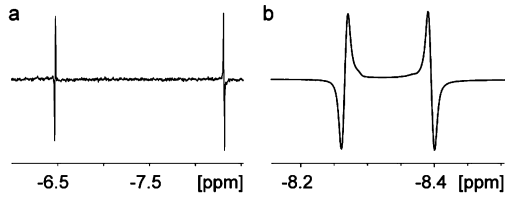

Figure 4. Single-laser shot, single 90° rf pulse, *para*-H_2 enhanced $^1H\{^{31}P\}$ NMR spectra of the hydride region of (a) **1** with τ = 0.05 ms (broadband ^{31}P decoupling) and (b) **2** with τ = 15 ms (selective ^{31}P decoupling of axial phosphorus).

spectrum of **1** in Figure 4a was acquired with a 90° rf pulse (13.5 μs), τ = 0.05 ms, and broadband ^{31}P decoupling. It shows two antiphase hydride signals at δ −6.47 and δ −8.30 where J_{HH} is resolved. The $^1H\{^{31}P\}$ NMR spectrum of **2** in Figure 4b was acquired with a 90° rf pulse (13.5 μs), τ = 15 ms, and selective ^{31}P decoupling of the axial phosphorus environment. It shows two antiphase hydride signals at δ −8.33 that are separated by a splitting equal to the difference in scalar coupling, $|J(PH)_{trans} - J(PH)_{cis}|$ = 83 Hz. Both of these spectra demonstrate enhanced signal intensity relative to the corresponding thermally polarized ^1H NMR spectra. The strength of this signal relative to the normal thermally polarized hydride trace is quantified later in the manuscript.

It is possible to use chemical-shift imaging to correlate the vertical position within the sample tube to the chemical-shift encoded molecular response. This method uses an incremented magnetic field gradient, applied along the z axis, to encode spatial position into the NMR signal. When undertaken in conjunction with photolysis, we can map the PHIP-derived signal enhancement onto this displacement axis. The spatially resolved NMR spectrum collected in this way is shown in Figure 5. It reveals that the hyperpolarized NMR signals for **2** are localized within a 3.2 mm region of the NMR tube. This measurement clearly highlights the region where UV-excitation takes place and therefore allows for the spatial differentiation of thermal and photochemical reactivity. In this case, **2** does not undergo thermal exchange with *para*-H_2 at 298 K, so there is no observed hyperpolarization of the hydride resonances outside of the laser-irradiated region of the NMR tube. Consequently, we can clearly state that the hydride signals we detect using the laser pump−NMR probe approach are all the result of the photochemical step.

The evolution of the photochemically generated NMR signals for **1** and **2** was investigated as a function of the pump−probe delay. A time sequence was recorded by measuring a series of $^1H\{^{31}P\}$ pump−probe NMR spectra for different values of τ, each employing one laser pulse and one rf pulse as shown in Figure 2b. This series of spectra encodes the evolution of the magnetic states that takes place during the pump−probe delay into the hydride signal intensity and can be readily interpreted by either looking at each spectrum in turn or following the change in integrated signal intensity of the hydride resonances. Using the latter approach, we find that the

dx.doi.org/10.1021/ja504732u | J. Am. Chem. Soc. 2014, 136, 10124−10131

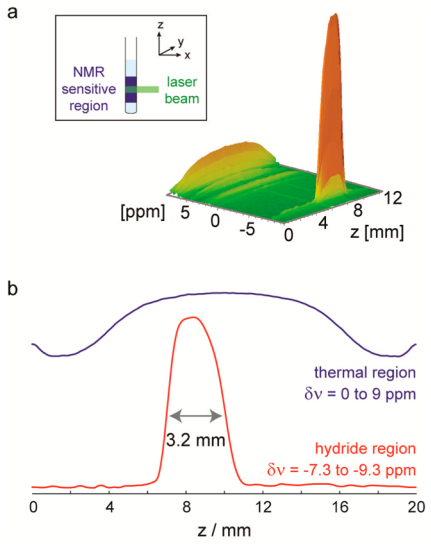

Figure 5. (a) Three-dimensional plot of signal intensity (vertical axis) vs chemical shift (ppm) and vertical displacement (mm) relative to the base of the NMR coil for **2**. (b) Projections of thermal signal intensity (0−9 ppm, blue) and the enhanced hydride signal intensity (−7.3 to −9.3 ppm, red) onto the vertical axis of the NMR tube.

integrals of the hydride signals of **1** exhibit an increase in intensity out to 200 μs, with an apparent rise time of ca. 70 μs (Figure 6a). Parallel kinetic measurements by UV spectroscopy exhibit a much more rapid 1.4 μs rise time,[58] thereby demonstrating that the reformation of **1** is much faster than this buildup of enhanced NMR signal. Further increase of τ as shown in Figure 6b reveals that this rise actually forms the initial part of a sinusoidal oscillation.

This change in signal amplitude can be readily understood if we consider the effect of the 90° rf pulse, which rotates $2I_zS_z$ and ZQ_x into unobservable zero-quantum and double-quantum terms while rotating ZQ_y (Figure 1b) into observable single-quantum terms (see section 2.2). The observed oscillation in hydride signal amplitude as a function of τ is therefore due to the periodic evolution that connects the initial ZQ_x state to the ZQ_y state, which proceeds under the influence of the difference in chemical shifts between the two hydrides or the difference in J coupling between the hydrides and a third nucleus (see section 2.2). We emphasize that even though the initial x−y coherence is created chemically, rather than with a radio frequency pulse, it still leads to a diagnostic signal in this experiment. A fit of this NMR signal to an exponentially decaying sine wave yields a frequency of 1101 ± 3 Hz (Figure 6b), in good agreement with the chemical shift difference, 1098 Hz, observed in the thermally polarized NMR spectrum of **1**.

In a classic 2D NMR experiment, a magnetic coherence is first created; next it is allowed to evolve during a variable delay before it is ultimately recorded as a free induction decay (FID). Fourier transformation then produces a 2D spectrum where the second dimension displays the information encoded during the evolution period. Here we used the same procedure to obtain 2D pump−probe NMR spectra, where the photochemically created magnetic coherence is also prepared with phase coherence. This is allowed to evolve during a variable pump−probe delay, τ, and is then recorded as an FID following a 90° rf pulse. This 2D approach is made possible by the reproducibility of the laser pump step and the synchronization with the NMR probe step. Figure 6c presents a 2D ^{1}H pump−probe NMR

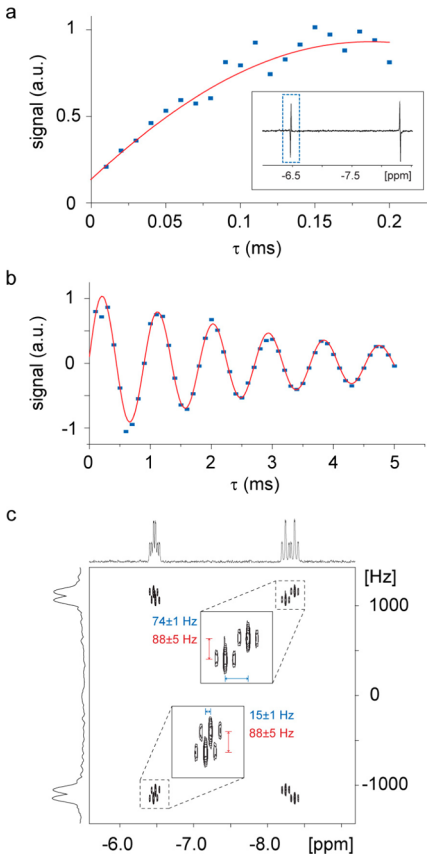

Figure 6. (a) Hydride signal integral versus τ for ^{1}H{^{31}P} NMR spectra of **1** (1×10^{-3} M, 3 atm *para*-H_2). Blue, experimental points; red line, exponentially decaying sine wave of 1101 ± 3 Hz generated using the fit parameters from panel b (inset trace illustrates the spectrum at τ = 0.05 ms). (b) Analogous ^{1}H{^{31}P} hydride signal integrals out to 5 ms. Red line, fit to exponentially decaying sine wave of 1101 ± 3 Hz. (c) 2D ^{1}H pump−probe NMR spectrum of **1** where the vertical dimension corresponds to evolution during τ. Inset shows 2× zoomed view.

spectrum of **1** acquired by varying τ from 0 to 14 ms in steps of 0.35 ms. In this spectrum, which was acquired without ^{31}P decoupling, we observe peaks at $\pm\Delta\delta$ = 1103 ± 3 Hz due to the evolution between ZQ_x and ZQ_y under the influence of the difference in hydride chemical shift. An additional splitting occurs due to evolution under the influence of the difference in J coupling between the hydride ligands and the equatorial phosphorus nucleus, $|J(PH)_{trans} - J(PH)_{cis}| = 88 \pm 5$ Hz (89 Hz in the 1D spectrum).

The related complex *cis*-Ru(dppe)$_2$(H)$_2$ (**2**) (Figure 3) is more complicated than **1** having chemically equivalent but magnetically inequivalent hydride ligands (AA′) that form an AA′XX′Y$_2$ spin system; X and Y are equatorial and axial ^{31}P nuclei, respectively. Normally, the hydride ligands of **2** yield a complex 36-component multiplet (Figure 7a) at δ −8.33 that simplifies to a pseudo-doublet separated by $|J(PH)_{trans} + J(PH)_{cis}| = 53$ Hz upon decoupling Y (Figure 7b).[61] When this complex is monitored by pump−probe NMR spectroscopy with *para*-H_2, both its hydride and equatorial ^{31}P signals (X) are observed to be hyperpolarized. Strikingly, the hydride signal now appears as a deceptively simple antiphase doublet of triplets due to the enhanced intensity of a subset of the 36 expected transitions (Figure 7c). The enhanced transitions reflect those nuclear spin states that are overpopulated by the

dx.doi.org/10.1021/ja504732u | J. Am. Chem. Soc. 2014, 136, 10124−10131

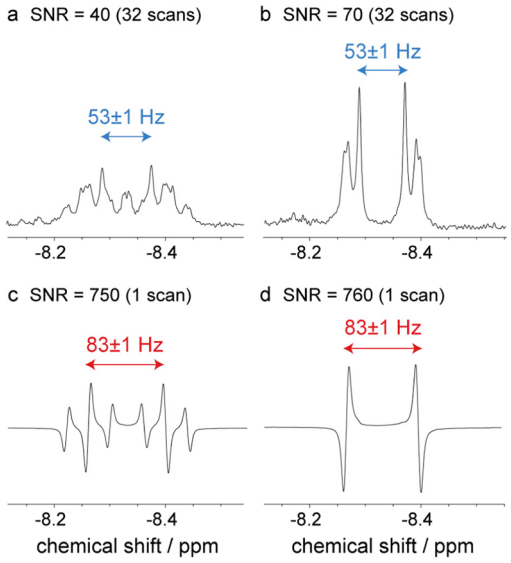

Figure 7. Thermal ^{1}H NMR spectra of **2**: (a) fully coupled and (b) with selective axial ^{31}P decoupling of the same sample. Pump–probe ^{1}H NMR spectra (90° rf pulse, τ = 15 ms) of **2**: (c) fully coupled and (d) with selective axial ^{31}P decoupling. The signal-to-noise ratios (SNR) are also shown.

evolution of the initial singlet state of the *para*-H_2-derived ^{1}H nuclei. The resulting dramatically simplified doublet feature is separated by $|J(PH)_{trans} - J(PH)_{cis}|$ = 83 Hz, and a splitting of 23 Hz due to axial ^{31}P interactions is visible. These measurements therefore reveal that $J(PH)_{trans}$ is ±68 Hz with $J(PH)_{cis}$ restricted to ∓15 Hz; decoupling of the axial ^{31}P-nuclei (Y) yields $J(HH)$ = 6 Hz as the antiphase splitting (Figure 7d). The NMR spectra in Figure 7 demonstrate that the hyperpolarized signals derived from a single FID can be detected with ^{1}H NMR signal-to-noise ratios of ca. 750:1, which compare with those of 45:1 for 32 scans under thermal conditions. This equates to the ready detection of ca. 10 nmol of material in a single transient.

Density matrix simulations of the hyperpolarized ^{1}H NMR spectra of **1** and **2** are presented in the Supporting Information (Figure S5) to support these deductions. The couplings and chemical shifts obtained from these simulations were in agreement with those obtained using standard NMR characterization methods (Figures S1 and S2, Supporting Information).

The hydride signals of **2** also oscillate in amplitude as the pump–probe delay τ is varied (Figure S4, Supporting Information). The resulting 2D ^{1}H pump–probe NMR spectrum of **2** (Figure 8a) reveals that this oscillation now has frequency ±83 ± 5 Hz and matches the difference between the *cis* and *trans* J couplings of the hydrides to the equatorial ^{31}P nuclei ($|J(PH)_{trans} - J(PH)_{cis}|$). Hence the hydride–phosphorus couplings of **2** play an analogous role to the hydride chemical shift difference in **1** in causing evolution of the ZQ_x term. In addition to this ^{1}H hyperpolarization, the equatorial ^{31}P nuclei (δ 65.7) of **2** become hyperpolarized, as shown by the 2D ^{31}P pump–probe spectrum in Figure 8b, which was acquired with 90° rf excitation and subsequent detection on the phosphorus channel. The axial phosphorus nuclei (δ 79.6) are, however, not hyperpolarized under these conditions because the difference in their couplings to the hydrides ($J(P_{ax}H_A) - J(P_{ax}H_B)$) is effectively zero.

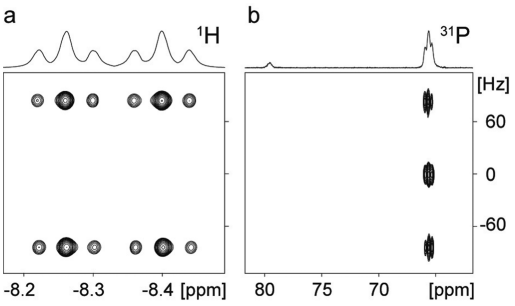

Figure 8. Two-dimensional pump–probe NMR spectra of **2** where the vertical dimension corresponds to evolution during τ and (a) ^{1}H is recorded or (b) ^{31}P is monitored.

2.2. Analysis of Evolution of Magnetization. In these NMR pump–probe experiments, the photodissociation of the two hydride ligands occurs within the laser pulse.[57] Hydrogen readdition from the *para*-H_2 reservoir (3 atm) then occurs following the laser pulse, on a time scale of a few microseconds.[57,58] Therefore, the *para*-H_2-derived ^{1}H nuclei initially retain their relative spin orientations and can be described by the singlet state: $-{}^{1}/_{2}(2I_zS_z + 2I_xS_x + 2I_yS_y)$.[11] It is noteworthy that, unlike more conventional PASADENA *para*-H_2 experiments where only the longitudinal two-spin order term, $2I_zS_z$, is preserved, here we benefit from the survival of the zero-quantum term, $ZQ_x = {}^{1}/_{2}(2I_xS_x + 2I_yS_y)$. This is a consequence both of the coherent way in which we initiate the readdition step and the reaction rate, which is fast relative to the evolution of the ZQ_x coherence. If the hydrides are chemically inequivalent ($\delta\nu \neq 0$), this ZQ_x term evolves during the pump–probe delay (τ) into a ZQ_y coherence: $ZQ_y = {}^{1}/_{2}(2I_yS_x - 2I_xS_y)$, under the application of the operator $(2\pi\delta\nu t){}^{1}/_{2}(I_z - S_z)$, as demonstrated by eq 1.[43] Similarly, a difference between the J couplings of the two hydrides (I and S) to a third nucleus, T, ($J_{IT} - J_{ST} \neq 0$) will result in the evolution of ZQ_x into $2ZQ_yT_z$ under the influence of the operator $((\pi/2)(J_{IT} - J_{ST})\tau)2(I_z - S_z)T_z$, as shown by eq 2. These evolutions serve two important functions in the pump–probe experiment. First, the evolution of ZQ_x into ZQ_y produces a detectable magnetic state from the initial NMR-silent singlet state. Second, the evolution frequencies encode important diagnositc information into the NMR response.

$$ZQ_x \xrightarrow{(2\pi\delta\nu t)\frac{1}{2}(I_z - S_z)} ZQ_x \cos(2\pi\delta\nu t) + ZQ_y \sin(2\pi\delta\nu t) \quad (1)$$

$$ZQ_x \xrightarrow{(\frac{\pi}{2}(J_{IT} - J_{ST})\tau)2(I_z - S_z)T_z} ZQ_x \cos(\pi(J_{IT} - J_{ST})\tau) + 2ZQ_yT_z \sin(\pi(J_{IT} - J_{ST})\tau) \quad (2)$$

At the end of the τ evolution period, prior to the application of the rf pulse, the state of the system will contain contributions from the longitudinal two-spin-order term as well as the zero-quantum coherence terms: ZQ_x and ZQ_y. Upon application of a broadband (i.e., nonselective) pulse, which rotates both of the ^{1}H nuclei by an angle, θ, all of these terms will give rise to NMR-observable magnetic states according to eq 3 (single-quantum states only).

dx.doi.org/10.1021/ja504732u | J. Am. Chem. Soc. 2014, 136, 10124–10131

$$\frac{1}{2}(2I_zS_z) \xrightarrow{\theta(I_y+S_y)} \frac{1}{2}(2I_xS_z + 2I_zS_x)\frac{1}{2}\sin 2\theta$$
$$ZQ_x \xrightarrow{\theta(I_y+S_y)} -\frac{1}{2}(2I_xS_z + 2I_zS_x)\frac{1}{2}\sin 2\theta$$
$$ZQ_y \xrightarrow{\theta(I_y+S_y)} -\frac{1}{2}(2I_yS_z - 2I_zS_y)\sin\theta \quad (3)$$

First, we note that the ZQ_x and longitudinal two-spin-order terms give rise to the same single-quantum states but with opposite signs. This means that observable NMR signal can only be obtained from these terms if their amplitudes differ and $\theta \neq 90°$. Second, inspection of eq 3 shows that a 90° pulse will in fact generate observable signal exclusively from the ZQ_y coherence, while other pulse rotation angles, such as 45°, can be used to detect contributions from the other states, particularly the longitudinal two-spin-order term $(2I_zS_z)$. All of the spectra reported here were measured with a 90° pulse and so show exclusively the evolution of ZQ_y during τ. This contrasts with a traditional PHIP experiment, where a 45° pulse is used because only the longitudinal two-spin-order term, $2I_zS_z$, is present, and it produces the maximum detectable response.[30]

The oscillation observed in the $^1H\{^{31}P\}$ spectra of **1** (Figure 6b) is completely described by eq 1. The 2D ^1H pump−probe spectrum of **1** in Figure 6c can be understood through the application of both eqs 1 and 2 to the initial ZQ_x state. Because the longitudinal two-spin-order term does not evolve during the pump−probe delay and is not observed with a 90° rf pulse, it is not considered further in this discussion. For the case of chemically inequivalent hydrides, the evolution due to the chemical shift and J coupling terms can be considered sequentially. As the pump−probe delay is changed, eq 1 shows that there will be a sinusoidal oscillation in the amplitude of the probed ZQ_y state, where the oscillation frequency is equal to the chemical-shift difference ($\delta\nu$ = 1098 Hz in **1**). In a 2D spectrum, this will correspond to peaks at $\pm\delta\nu$ in the indirect (τ) evolution dimension. According to eq 2, there will be an additional oscillation due to the difference in the *trans* and *cis* J couplings between the hydrides and the in-plane phosphorus nucleus, $\Delta J = |J(PH)_{trans} - J(PH)_{cis}| = 89$ Hz. This oscillation will produce a further splitting in the indirect (τ) evolution dimension of the 2D spectrum with peaks at $\delta\nu + {}^1/_2\Delta J$ and $\delta\nu - {}^1/_2\Delta J$. This is precisely what is observed in Figure 6c.[62] In addition, the form of the hyperpolarized ^1H NMR spectrum in the direct dimension can be interpreted in a straightforward way. Each hydride gives rise to an antiphase doublet of triplets, where the antiphase splitting is equal to the homonuclear hydride−hydride coupling, the doublet splitting is equal to the equatorial $^{31}P-^1H$ coupling, and the triplet splitting is equal to the axial $^{31}P-^1H$ coupling.

In complex **2**, the hydrides are chemically equivalent but magnetically inequivalent, so there is no evolution due to the chemical shift terms, as shown by eq 1. Equation 2 describes the evolution of ZQ_x when two magnetically inequivalent nuclei are coupled to a single third nucleus. The presence of two equatorial ^{31}P nuclei (T and R) in **2** can therefore be analyzed by the application of eq 2 twice in succession (once for the coupling to T and once for the coupling to R, where R replaces T in eq 2) leading to an effective oscillation frequency of ΔJ and peaks in the 2D ^1H pump−probe spectrum at $+\Delta J$ and $-\Delta J$ (Figure 8a). Although this approach does not take into account the effect of the strong coupling of the AA′XX′ system, it is sufficient to provide an intuitive understanding of the peaks in the 2D ^1H pump−probe spectrum. In contrast, inclusion of strong coupling is required to explain the observed hyperpolarization of the equatorial ^{31}P nuclei in Figure 8b. The $^1H-^{31}P$ coupled state generated by eq 2, $2ZQ_yT_z$, does not yield any observable single-quantum states following the application of an rf pulse on the phosphorus channel. Therefore, magnetic states of this type cannot account for the observed ^{31}P hyperpolarization in the 2D ^{31}P pump−probe spectrum in Figure 8b. However, in the strong coupling regime the coupled state, $2ZQ_yT_z$, will evolve into $2(I_z - S_z)T_z$ under the influence of the nonsecular part of the $^1H-^1H$ J-coupling interaction, $\pi J_{IS}(2I_xS_x + 2I_yS_y)$, as demonstrated by eq 4.[43]

$$2ZQ_yT_z \xrightarrow{\pi J_{IS}(2I_xS_x+2I_yS_y)\tau} 2ZQ_yT_z\cos(2\pi J_{IS}\tau) + \frac{1}{2}2(I_z - S_z)T_z\sin(2\pi J_{IS}\tau) \quad (4)$$

It is this $2(I_z - S_z)T_z$ state that gives rise to the ^{31}P NMR signals observed following the application of an rf pulse to the phosphorus channel in the 2D ^{31}P pump−probe spectrum in Figure 8b. While transfer from *para*-H_2-derived ^1H nuclei to a heteronucleus has been achieved previously in combination with rf irradiation[63] or in the low-field regime,[64,65] this is an example of spontaneous transfer of *para*-H_2 hyperpolarization to a heteronucleus in the high field regime.

3. CONCLUSION

In this paper, we have demonstrated that NMR spectroscopy can be used in a laser pump−NMR probe mode to access microsecond to millisecond time scale events in an approach analogous to other laser based time-resolved spectroscopies. Our measurements were made possible by combining laser-synchronized chemical initiation with *para*-H_2 hyperpolarization. Crucially, in the pumping stage of the experiment, $x-y$ coherence is created through a chemical reaction that proceeds on a microsecond time scale. This $x-y$ coherence responds to the molecular environment as manifested in both the 1D spectra and the oscillatory evolution of the spectra as a function of the pump−probe delay. This chemically generated coherence contrasts with the normal situation for NMR spectroscopy where $x-y$ coherences are the direct result of a radio frequency pulse. Furthermore, this method differs significantly from traditional *para*-H_2 methods of PASADENA and ALTADENA, which lack a synchronous initiation step and hence only yield time-averaged magnetic states prior to rf excitation.[44] For example, when transition metal complexes are examined, the oscillations of the zero quantum coherence are obscured because of the asynchronous H_2 cycling (multiple H_2 addition and elimination). Similarly, multiple asynchronous catalytic steps normally cause time-averaging in instances where hydrogenation products are formed irreversibly.

In the two cases illustrated here, $Ru(PPh_3)_3(CO)(H)_2$ (**1**) and *cis*-$Ru(dppe)_2(H)_2$ (**2**), the signals oscillate for different reasons. In the case of **1**, it is the creation of two chemically inequivalent hydrides that leads to an oscillation of frequency, 1101 ± 3 Hz corresponding to their chemical shift difference. For **2**, however, it is magnetic inequivalence that results in a smaller oscillation frequency of 83 ± 5 Hz corresponding to a difference in spin−spin coupling, $|J(PH)_{trans} - J(PH)_{cis}|$. This approach therefore readily differentiates the spin topology of the product and is applicable to compounds with either chemical inequivalence or magnetic inequivalence via differ-

ences in *J*-coupling. We have also demonstrated that we can monitor changes in the spectra observed with successive pump−probe delays differing from one another by 10 μs. The rise time of the oscillations sets an upper limit for the formation of the product that is measured as 70 μs in the case of **1**. The time scale of our experiments is defined by the frequency difference between the two hydride resonances in the case of **1** and by the difference in spin−spin coupling in the case of **2**.

The sensitivity of the method is illustrated by single scans with signal-to-noise ratios as high as 750:1 that detect nanomole amounts of product. The potential of this method as a diagnostic probe for photoinduced reactions is further demonstrated by chemical-shift imaging combined with laser irradiation that can differentiate thermal and photochemical reactivity *in situ* within the time frame of the experiment.

We are currently working to develop a full theoretical framework and optimize the experimental parameters so as to extend the method to other types of reaction products that have been observed with *para*-H_2 hyperpolarization.[28] In the future, we seek to exploit its remarkable potential to quantify chemical kinetics on a microsecond time scale while simultaneously benefiting from the structural information provided by NMR detection. In principle, any system that can be initiated synchronously and sensitized with *para*-H_2 could be followed using our method. Another potential application of this technique is as a test-bed for NMR pulse sequences designed to manipulate long-lived singlet states.

4. EXPERIMENTAL SECTION

All NMR spectra were recorded on a Bruker Avance widebore 600 MHz spectrometer fitted with a BBO probe. Laser photolysis was carried out with a pulsed Nd:YAG laser (Continuum Surelite II) fitted with a frequency tripling crystal (output 355 nm). Operating conditions were typically: 10 Hz repetition rate, flash lamp voltage 1.49 kV, and Q-switch delay increased from the standard to 320 ms yielding a laser power of 85 mW. The unfocused laser beam is directed at the base of the spectrometer and reflected up into the probe via a mirror (Figure 2a). Adjustment screws control the vertical and horizontal position of the mirror, which is on a kinematic mount. The system is fully shielded from the operator, and the screws of the kinematic mount can be adjusted from outside the shield. The laser radiation is incident on a fixed mirror that is level with the sample and passes through a hole in the probe onto the NMR tube. Standard NMR tubes fitted with Young's taps were used. The samples contained 1−2 mg of compound and approximately 0.4 mL of solvent. A sample of **2** in C_6D_6 was used for laser alignment with *para*-H_2 amplification in real time.

Standard NMR pulse sequences were modified for use with *para*-H_2 by including a synchronized laser initiation sequence prior to NMR excitation (Figure 2b). A purpose-written program was used to control the laser firing from the NMR console with the laser set on external triggering. The fire signals are sent to the laser via a BNC cable. The program sets the laser to fire three warm-up shots before opening the shutter for the fire signal. The NMR pulse is initiated at a set delay time (τ) following the fire signal. The intrinsic time delay between sending the fire signal from the spectrometer and the actual firing of the laser pulse was measured with a photodiode and an oscilloscope to be 140 μs. This signal delay was incorporated into the pulse sequence such that synchronized measurements with a time delay, τ, were achieved by setting the spectrometer delay to τ + 140 μs. The precision of this delay between the laser and rf pulses is controlled by the 200 ns clock of the spectrometer.

Two-dimensional pump−probe NMR experiments were carried out by acquiring a series of 1D spectra in which the delay between the laser pulse and the rf excitation, τ, was incremented in the usual way to assemble a 2D data set. This 2D data set was subsequently Fourier transformed under magnitude mode to generate 2D spectra such as those presented in Figures 6c and 8.

Chemical-shift imaging (CSI) was used to correlate the vertical position within the sample tube to chemical shift (Figure 5). The CSI method used here employs an incremented magnetic field gradient along the *z*-axis to encode spatial information into the phase of the detected signals. Subsequent Fourier transformation of the 2D data set gives a chemical shift spectrum in the directly observed dimension (F2) and position in the indirect evolution dimension (F1). The pulse sequence used for chemical-shift imaging is shown in the Supporting Information (Figure S3). The maximum gradient strength used is dependent on the number of increments and the length and shape of the gradient pulse. For the ^{1}H experiments, we used 1 ms half-sine gradient pulses, with maximum strength of 5.99 G/cm, and 64 data points in the second dimension. This corresponds to a field of view of 2 cm (Figure S6, Supporting Information). A two-step phase cycle of the 180° pulse was used to remove artifacts in the image.

■ ASSOCIATED CONTENT

Supporting Information

NMR characterization data, additional spectra with simulations, and further technical descriptions. This material is available free of charge via the Internet at http://pubs.acs.org.

■ AUTHOR INFORMATION

Corresponding Authors

simon.duckett@york.ac.uk
robin.perutz@york.ac.uk

Notes

The authors declare no competing financial interest.

■ ACKNOWLEDGMENTS

We are grateful for support to EPSRC (grant EP/K022792/1), the Ministerio de Ciencia e Innovación and the Fundación Española para la Ciencia y la Tecnología (OT), and the Spanish MEC Consolider Ingenio 2010-ORFEO−CSD2007-00006 research programme (BE). Catherine Sexton, Sarah Henshaw, and Pedro Aguiar provided experimental help.

■ REFERENCES

(1) Mann, B. E. In *Encyclopedia of Nuclear Magnetic Resonance*; Grant, D. M., Harris, R. K., Eds.; Wiley: Chichester, U.K., 1996; p 3400.
(2) Perrin, C. L.; Dwyer, T. J. *Chem. Rev.* **1990**, *90*, 935.
(3) Bart, J.; Kolkman, A. J.; Oosthoek-de Vries, A. J.; Koch, K.; Nieuwland, P. J.; Janssen, H.; van Bentum, P. J. M.; Ampt, K. A. M.; Rutjes, F. P. J. T.; Wijmenga, S. S.; Gardeniers, H.; Kentgens, A. P. M. *J. Am. Chem. Soc.* **2009**, *131*, 5014.
(4) Wagner, G. E.; Sakhaii, P.; Bermel, W.; Zangger, K. *Chem. Commun.* **2013**, *49*, 3155.
(5) Zewail, A. H. *Angew. Chem., Int. Ed.* **2000**, *39*, 2587.
(6) Zhang, R.; Newcomb, M. *Acc. Chem. Res.* **2008**, *41*, 468.
(7) Butler, J. M.; George, M. W.; Schoonover, J. R.; Dattelbaum, D. M.; Meyer, T. J. *Coord. Chem. Rev.* **2007**, *251*, 492.
(8) Kukura, P.; McCamant, D. W.; Mathies, R. A. *Annu. Rev. Phys. Chem.* **2007**, *58*, 461.
(9) Nibbering, E. T. J.; Fidder, H.; Pines, E. *Annu. Rev. Phys. Chem.* **2005**, *56*, 337.
(10) Browne, W. R.; McGarvey, J. J. *Coord. Chem. Rev.* **2007**, *251*, 454.
(11) Anwar, M. S.; Blazina, D.; Carteret, H. A.; Duckett, S. B.; Halstead, T. K.; Jones, J. A.; Kozak, C. M.; Taylor, R. J. K. *Phys. Rev. Lett.* **2004**, *93*, No. 040501.
(12) Calladine, J. A.; Torres, O.; Anstey, M.; Ball, G. E.; Bergman, R. G.; Curley, J.; Duckett, S. B.; George, M. W.; Gilson, A. I.; Lawes, D. J.; Perutz, R. N.; Sun, X.-Z.; Vollhardt, K. P. C. *Chem. Sci.* **2010**, *1*, 622.

(13) Ampt, K. A. M.; Duckett, S. B.; Perutz, R. N. *Dalton Trans.* **2007**, 2993.
(14) Schroder, L.; Lowery, T. J.; Hilty, C.; Wemmer, D. E.; Pines, A. *Science* **2006**, *314*, 446.
(15) Happer, W. *Rev. Mod. Phys.* **1972**, *44*, 169.
(16) Garimella, P. D.; Meldrum, T.; Witus, L. S.; Smith, M.; Bajaj, V. S.; Wemmer, D. E.; Francis, M. B.; Pines, A. *J. Am. Chem. Soc.* **2014**, *136*, 164.
(17) Ardenkjaer-Larsen, J. H.; Fridlund, B.; Gram, A.; Hansson, G.; Hansson, L.; Lerche, M. H.; Servin, R.; Thaning, M.; Golman, K. *Proc. Natl. Acad. Sci. U. S. A.* **2003**, *100*, 10158.
(18) Müller-Warmuth, W.; Meise-Gresch, K. *Adv. Magn. Reson.* **1983**, *11*, 1.
(19) Schäublin, S.; Wokaun, A.; Ernst, R. R. *J. Magn. Reson.* **1977**, *27*, 273.
(20) Trease, D.; Bajaj, V. S.; Paulsen, J.; Pines, A. *Chem. Phys. Lett.* **2011**, *503*, 187.
(21) Goez, M.; Kuprov, I.; Mok, K. H.; Hore, P. J. *Mol. Phys.* **2006**, *104*, 1675.
(22) Harper, S. M.; Neil, L. C.; Day, I. J.; Hore, P. J.; Gardner, K. H. *J. Am. Chem. Soc.* **2004**, *126*, 3390.
(23) Kiryutin, A. S.; Morozova, O. B.; Kuhn, L. T.; Yurkovskaya, A. V.; Hore, P. J. *J. Phys. Chem. B* **2007**, *111*, 11221.
(24) Mok, K. H.; Nagashima, T.; Day, I. J.; Jones, J. A.; Jones, C. J. V.; Dobson, C. M.; Hore, P. J. *J. Am. Chem. Soc.* **2003**, *125*, 12484.
(25) Perrier, S.; Mugeniwabagara, E.; Kirsch-De Mesmaeker, A.; Hore, P. J.; Luhmer, M. *J. Am. Chem. Soc.* **2009**, *131*, 12458.
(26) Schaublin, S.; Wokaun, A.; Ernst, R. R. *Chem. Phys.* **1976**, *14*, 285.
(27) Duckett, S. B.; Mewis, R. E. *Acc. Chem. Res.* **2012**, *45*, 1247.
(28) Green, R. A.; Adams, R. W.; Duckett, S. B.; Mewis, R. E.; Williamson, D. C.; Green, G. G. R. *Prog. Nucl. Magn. Reson. Spectrosc.* **2012**, *67*, 1.
(29) Bowers, C. R.; Weitekamp, D. P. *Phys. Rev. Lett.* **1986**, *57*, 2645.
(30) Bowers, C. R.; Weitekamp, D. P. *J. Am. Chem. Soc.* **1987**, *109*, 5541.
(31) Pravica, M. G.; Weitekamp, D. P. *Chem. Phys. Lett.* **1988**, *145*, 255.
(32) Eisenschmid, T. C.; Kirss, R. U.; Deutsch, P. P.; Hommeltoft, S. I.; Eisenberg, R.; Bargon, J.; Lawler, R. G.; Balch, A. L. *J. Am. Chem. Soc.* **1987**, *109*, 8089.
(33) Lopez-Serrano, J.; Duckett, S. B.; Aiken, S.; Lenero, K. Q. A.; Drent, E.; Dunne, J. P.; Konya, D.; Whitwood, A. C. *J. Am. Chem. Soc.* **2007**, *129*, 6513.
(34) Godard, C.; Duckett, S. B.; Henry, C.; Polas, S.; Toose, R.; Whitwood, A. C. *Chem. Commun.* **2004**, 1826.
(35) Permin, A. B.; Eisenberg, R. *J. Am. Chem. Soc.* **2002**, *124*, 12406.
(36) Giernoth, R.; Huebler, P.; Bargon, J. *Angew. Chem., Int. Ed.* **1998**, *37*, 2473.
(37) Viale, A.; Santelia, D.; Napolitano, R.; Gobetto, R.; Dastru, W.; Aime, S. *Eur. J. Inorg. Chem.* **2008**, 4348.
(38) Bhattacharya, P.; Harris, K.; Lin, A. P.; Mansson, M.; Norton, V. A.; Perman, W. H.; Weitekamp, D. P.; Ross, B. D. *Magn. Reson. Mater. Phys. Biol. Med.* **2005**, *18*, 245.
(39) Bouchard, L.-S.; Burt, S. R.; Anwar, M. S.; Kovtunov, K. V.; Koptyug, I. V.; Pines, A. *Science* **2008**, *319*, 442.
(40) Adams, R. W.; Aguilar, J. A.; Atkinson, K. D.; Cowley, M. J.; Elliott, P. I. P.; Duckett, S. B.; Green, G. G. R.; Khazal, I. G.; Lopez-Serrano, J.; Williamson, D. C. *Science* **2009**, *323*, 1708.
(41) Duckett, S. B.; Sleigh, C. J. *Prog. Nucl. Magn. Reson. Spectrosc.* **1999**, *34*, 71.
(42) Sorensen, O. W.; Eich, G. W.; Levitt, M. H.; Bodenhausen, G.; Ernst, R. R. *Prog. Nucl. Magn. Reson. Spectrosc.* **1983**, *16*, 163.
(43) Natterer, J.; Bargon, J. *Prog. Nucl. Magn. Reson. Spectrosc.* **1997**, *31*, 293.
(44) Natterer, J.; Schedletzky, O.; Barkemeyer, J.; Bargon, J.; Glaser, S. J. *J. Magn. Reson.* **1998**, *133*, 92.
(45) Levitt, M. H. *Annu. Rev. Phys. Chem.* **2012**, *63*, 89.
(46) Pileio, G.; Bowen, S.; Laustsen, C.; Tayler, M. C. D.; Hill-Cousins, J. T.; Brown, L. J.; Brown, R. C. D.; Ardenkjaer-Larsen, J. H.; Levitt, M. H. *J. Am. Chem. Soc.* **2013**, *135*, 5084.
(47) Feng, Y.; Davis, R. M.; Warren, W. S. *Nat. Phys.* **2012**, *8*, 831.
(48) Ahuja, P.; Sarkar, R.; Jannin, S.; Vasos, P. R.; Bodenhausen, G. *Chem. Commun.* **2010**, *46*, 8192.
(49) Carravetta, M.; Levitt, M. H. *J. Am. Chem. Soc.* **2004**, *126*, 6228.
(50) Franzoni, M. B.; Buljubasich, L.; Spiess, H. W.; Muennemann, K. *J. Am. Chem. Soc.* **2012**, *134*, 10393.
(51) Zhang, Y.; Soon, P. C.; Jerschow, A.; Canary, J. W. *Angew. Chem., Int. Ed.* **2014**, *53*, 3396.
(52) Calladine, J. A.; Duckett, S. B.; George, M. W.; Matthews, S. L.; Perutz, R. N.; Torres, O.; Khuong, Q. V. *J. Am. Chem. Soc.* **2011**, *133*, 2303.
(53) Ball, G. E.; Brookes, C. M.; Cowan, A. J.; Darwish, T. A.; George, M. W.; Kawanami, H. K.; Portius, P.; Rourke, J. P. *Proc. Natl. Acad. Sci. U. S. A.* **2007**, *104*, 6927.
(54) Glorius, F.; Altenhoff, G.; Goddard, R.; Lehmann, C. *Chem. Commun.* **2002**, 2704.
(55) Clark, J. L.; Duckett, S. B. *Dalton Trans.* **2014**, *43*, 1162.
(56) Eguillor, B.; Caldwell, P. J.; Cockett, M. C. R.; Duckett, S. B.; John, R. O.; Lynam, J. M.; Sleigh, C. J.; Wilson, I. *J. Am. Chem. Soc.* **2012**, *134*, 18257.
(57) Colombo, M.; George, M. W.; Moore, J. N.; Pattison, D. I.; Perutz, R. N.; Virrels, I. G.; Ye, T. Q. *J. Chem. Soc., Dalton Trans.* **1997**, 2857.
(58) Cronin, L.; Nicasio, M. C.; Perutz, R. N.; Peters, R. G.; Roddick, D. M.; Whittlesey, M. K. *J. Am. Chem. Soc.* **1995**, *117*, 10047.
(59) Campian, M. V.; Perutz, R. N.; Procacci, B.; Thatcher, R. J.; Torres, O.; Whitwood, A. C. *J. Am. Chem. Soc.* **2012**, *134*, 3480.
(60) Schott, D.; Callaghan, P.; Dunne, J.; Duckett, S. B.; Godard, C.; Goicoechea, J. M.; Harvey, J. N.; Lowe, J. P.; Mawby, R. J.; Muller, G.; Perutz, R. N.; Poli, R.; Whittlesey, M. K. *Dalton Trans.* **2004**, 3218.
(61) Gunther, H. *Angew. Chem., Int. Ed.* **1972**, *11*, 861.
(62) The difference in couplings between the hydrides and the axial phosphorus nuclei is very small (<5 Hz). While we would expect an additional splitting in the 2D spectrum due to this difference, it is not resolved in Figure 6c.
(63) Roth, M.; Koch, A.; Kindervater, P.; Bargon, J.; Spiess, H. W.; Munnemann, K. *J. Magn. Reson.* **2010**, *204*, 50.
(64) Goldman, M.; Johannesson, H. *C. R. Phys.* **2005**, *6*, 575.
(65) Hövener, J.-B.; Chekmenev, E. Y.; Harris, K. C.; Perman, W. H.; Robertson, L. W.; Ross, B. D.; Bhattacharya, P. *Magn. Reson. Mater. Phys. Biol. Med.* **2009**, *22*, 111.